ACS OMEGA

Open Access

http://pubs.acs.org/journal/acsodf

Article

The Production Splitting Method of Offshore Multilayer Combined Water Flooding Gas Wells with Gas Dissolving

Chaoqun Ren,* Chuanzhong Deng, Zhehao Jiang, Qiang Fu, Lili Jiang, Yuchuan Guo, and Keliu Wu

Cite This: *ACS Omega* 2024, 9, 12850−12865

Read Online

ACCESS | Metrics & More | Article Recommendations

ABSTRACT: Offshore gas reservoirs are characterized by thin interlayers, high production, few wells, etc., and are often exploited by multilayer combined mining, whereas the production dynamics of multilayer gas reservoirs are very different from those of single-layer gas reservoirs. Therefore, clarifying the gas production contribution of each layer in multilayer combined gas reservoirs is an important prerequisite for analyzing the potential of gas reservoirs and realizing efficient development. In this paper, unlike the past method of evaluating the gas production contribution of each layer by using the KH attribute of the reservoir, we combined the modified B−L equation considering CO_2 dissolution and the multilayer multizone seepage equation to establish a dynamic split model of the production dynamics of multilayer water-driven gas reservoirs, verified the reliability of the model through the numerical model and the results of the production well logging, quantitatively analyzed the degree of influence of each parameter on the contribution of the layered gas production, and designed the orthogonal experiments. The main controlling factors of the gas production contribution of each layer were determined. The results of the study show that (1) the main controlling factors for the gas production contribution of each layer in the early stage of WDG are, in order, permeability, thickness, outer boundary distance, porosity, CO_2 content, and total gas production rate; however, the main controlling factors for the gas production contribution of each layer in the late stage of WDG are, in order, thickness, permeability, outer boundary distance, porosity, CO_2 content, and total gas production rate; and the combined view shows that the permeability and thickness have the greatest influence. (2) In multilayer production, the conditions of high permeability, close gas−water boundary, poor gas content, and low CO_2 content will reduce the gas production contribution of the layer with the increase of production time. (3) Compared with the results of production logging and numerical simulation, the split model can better predict the gas production of each layer, and the prediction error is no more than 10%. (4) By comparing with the numerical simulation results, the model can realize the prediction of the time of seeing water in the layer with stronger water body capability. (5) The model takes into account the effect of the CO_2 content, better reflects the actual gas composition of each layer, and can improve the production prediction accuracy by up to 4%. Considering the high cost of production logging in offshore oil and gas fields, the inability of the KH method to reflect the dynamic changes of gas production in each layer, the poor application of stratified sampling to dry gas reservoirs, and other limitations, the model in this paper can be utilized to simulate the multilayer water-driven gas drive process when the energy of the water body is strong by using the geological parameters of the reservoir and the fluid parameters, and the simulation results of this model provide directions for offshore multilayer water-driven gas reservoirs to improve the recovery rate, and for plugging and regulating the water and exploiting the potential of gas wells that have seen water.

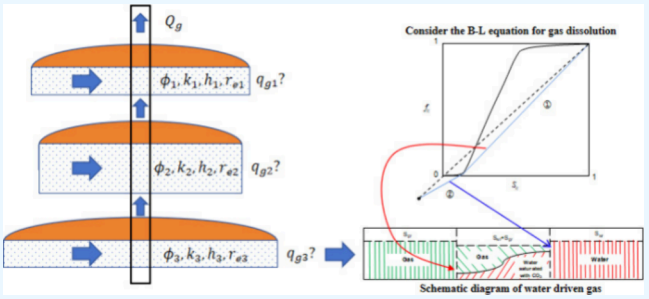

1. INTRODUCTION

Because of the characteristic of low well productivity, offshore gas reservoirs often adopt the method of multilayer joint production for exploitation. However, because of the high cost of offshore testing, it is difficult to frequently conduct production logging analysis for each small layer. The dynamic changes in the production ratio of each layer during the production process are not well understood because of the influence of various factors such as physical properties, reserves, and water invasion in multilayer joint production gas reservoirs. This leads to difficulties in accurately evaluating the remaining potential of gas field development, making it necessary to conduct research on methods for splitting well production among multiple layers. Scholars at home and abroad have conducted extensive research on pressure and production calculation issues during multilayer joint production. Currently,

Received: November 9, 2023
Revised: February 7, 2024
Accepted: February 9, 2024
Published: March 6, 2024

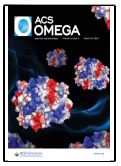

common methods include production logging, geochemical methods,[1] physical experiments,[2,3] numerical simulation, and mathematical statistical methods.[4] Among these methods, production logging has high implementation costs, is limited to only a few wells due to the influence of drill pipes, and has difficulty predicting long-term production dynamics. Geochemical methods require the reservoir to have condensate oil samples, whereas physical experiments are unable to describe the characteristics of the reservoir scale. Statistical methods lack clear physical significance The aforementioned methods have certain limitations. However, constructing a multilayer gas reservoir seepage model through theoretical modeling and solving for layered production can maximize the reflection of the physical laws behind oil and gas migration. This method is highly beneficial for tapping the potential of gas reservoirs and improving recovery rates. Lefkovits et al. were the first to initiate research on the contribution of layered production in multilayered closed reservoirs.[5] The result identified that early-stage production is affected by the flow coefficient, whereas late-stage production is influenced by the storage capacity ratio. Building on the work of Lefkovits et al., Tariq and Ramey developed a multilayered reservoir seepage model that takes into account well storage coefficient, skin effect, and constant rate production with varying radii, and numerical inversion was performed using Stefest's method to find the model solution in real space.[6] Shah and Spath utilized the Duhamel formula to perform a coupled solution for bottomhole pressure in multilayer reservoirs, thereby enhancing the methodology for solving multilayer reservoir pressures.[7] Jia derived a single-phase seepage model without crossflow for multilayer and multizone reservoirs, taking into account various boundary conditions for corresponding production and pressure solutions. This outcome provides a framework for determining production contributions from diverse complex formations.[8] Fankun et al. introduced a seepage resistance coefficient to modify the Buckley−Leverett equation in gas-drive oil and water-drive gas processes and introduced the multiple composite reservoir seepage theory to establish a mathematical model that can characterize the change in CO_2−water−gas alternating drive injection capacity.[9]

The existing multilayer seepage model does not give enough consideration to the water-driven gas process, especially the formation of water-driven gas transition zone, and only equates the role of water to the pressure supply boundary, and the model also lacks the consideration of the different components of the layered gas, and the change of temperature and pressure under the stratigraphic conditions will greatly affect the gas physical properties parameters. In this paper, we consider the modified B−L equation of gas dissolution, and introduce the gas characteristics affected by temperature and pressure into the seepage equation, establish the seepage model of multi-layer and multi-zone water-driven gas reservoirs, and equate the process of water-driven gas with water−water−gas transition zone-gas, and then carry out the dynamic production capacity prediction of multi-layer water-driven gas reservoirs, and quantitatively evaluate the influence of different parameters on the layered output contribution, summarize the quantitative relationship of the influence of parameters on the layered output contribution, and clarify the main layered output contribution of the parameters, and define the main layered output contribution of the water-driven gas reservoir. The quantitative evaluation of the influence of different parameters on the layered output contribution was carried out, and the quantitative relationship between the influence of each parameter on the layered output contribution was summarized.The detailed workflow is shown in Figure 1.

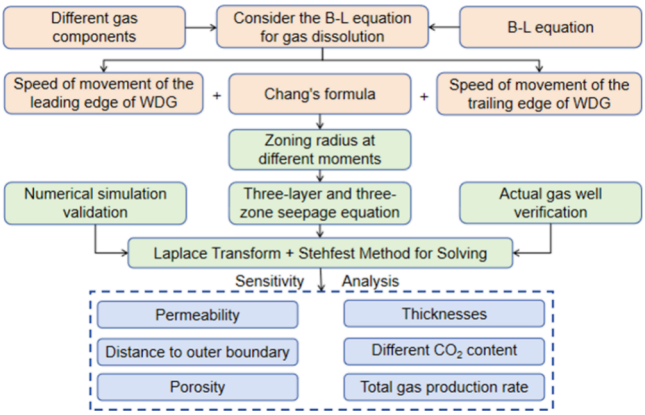

Figure 1. Workflow chart.

2. MULTILAYERED INTEGRATED WATER FLOODING GAS RESERVOIR MODEL

2.1. Physical Model. The model presented in this article assumes a multilayered water flooding gas reservoir with fixed pressure boundaries. Given the layered gas composition of the multiple gas reservoirs, the following fundamental assumptions have been made: (1) The geological formation is circular, horizontally homogeneous, and nonuniform in thickness. Impermeable layers exist between each small layer both above and below. A single production well is located at the center of the circular formation, producing gas at a constant flow rate. (2) The reservoir space contains a relatively high saturation of bound water, and the solubility of CO_2 in water is taken into account in the gas composition, without considering the diffusion of the water phase in the gas or rock reactions. (3) The energy of the surrounding water is sufficient, and the fluid is slightly compressible. The development process is isothermal, and flow follows Darcy's law while ignoring capillary forces and gravity. (4) The studied physical stage pertains to the period prior to the appearance of edge water in production wells, specifically the gas production phase during water flooding. The saturation profiles of multilayer water-flooded gas reservoirs are illustrated in Figure 2, where zones I, IV, and VII denote the gas zones; zones II, V, and VIII represent the gas−water transition zones; and zones III, VI, and IX correspond to the water zones.

2.2. Consider the B−L Equation for Gas Dissolution. This article refers to a one-dimensional CO_2 flooding model and establishes a one-dimensional water flooding nonpiston model based on it.[9] As an example, the B−L equation is modified. The mass concentration conservation equation for the CO_2 component in the form of flow rate is as follows:

$$\begin{cases} \dfrac{\partial C_{CO_2}}{\partial t_D} + \dfrac{\partial F_{CO_2}}{\partial x_D} = 0 \\ C_{CO_2} = S_g C_{CO_2,g} + (1 - S_g) C_{CO_2,w} \\ F_{CO_2} = f_g C_{CO_2,g} + (1 - f_g) C_{CO_2,w} \\ t_D = \dfrac{qBt}{qAL},\ x_D = \dfrac{x}{L} \end{cases} \quad (1)$$

https://doi.org/10.1021/acsomega.3c08949
ACS Omega 2024, 9, 12850−12865

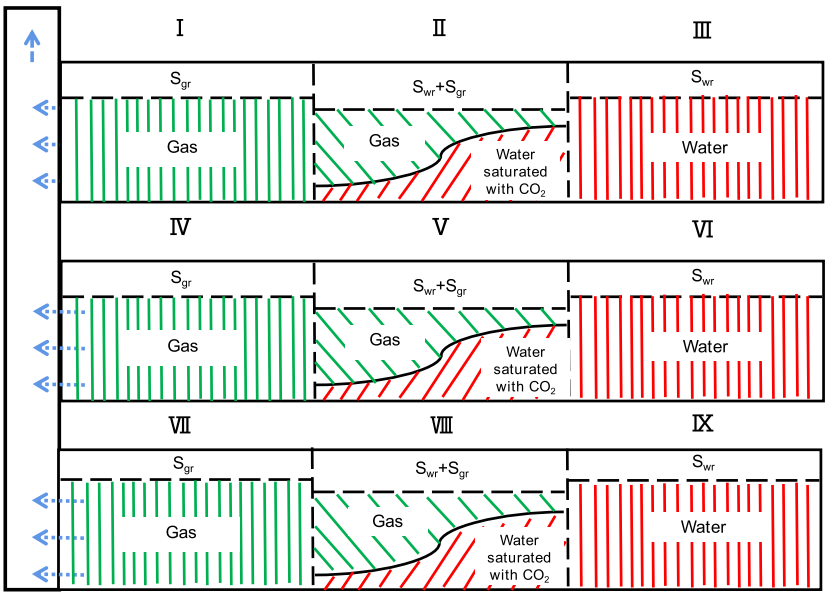

Figure 2. Schematic diagram of multilayer water flood saturation profile.

where the parameters and variables are defined in Appendix A. According to the above equation, the characteristic line method can be used to derive the velocities of the leading edges of water-driven gas $v_{CO_2,\,I-II}$ and trailing edges of water-driven gas $v_{CO_2,\,II-III}$, which are:

$$\begin{cases} V_{CO_2,I-II} \approx \dfrac{f_g^{II-} - D_{I-II}}{S_g^{II-} - D_{I-II}} = \left(\dfrac{df_g}{dS_g}\right)\Big|_{S_{g,I-II}} \\ V_{CO_2,II-III} \approx \dfrac{f_g^{II+} - D_{II-III}}{S_g^{II+} - D_{II-III}} = \left(\dfrac{df_g}{dS_g}\right)\Big|_{S_{g,II-III}} \\ D_{I-II} = \dfrac{C_{CO_{2,g}}^{I+} - C_{CO_{2,W}}^{II-}}{C_{CO_2,g}^{II-} - C_{CO_2,W}^{II-}},\ D_{II-III} = \dfrac{C_{CO_2,W}^{II+}}{C_{CO_2,W}^{II+} - C_{CO_2,g}^{II+}} \end{cases} \tag{2}$$

where the parameters and variables are defined in Appendix A.

In the equation, D_{I-II} and D_{II-III} define the seepage resistance coefficients between zone I and zone II as well as between zone II and zone III.

The equation above calculates the 1D velocity of the front and rear edges of water displacement by gas. It needs to be converted to planar radial flow to adapt to the derivation of more complex gas−water seepage equations later in the text. The planar radial flow velocity can be expressed as

$$\frac{R^2\pi h\varphi}{qBt}\Big|_{S_g} = \frac{df_g}{dS_g}\Big|_{S_g} \tag{3}$$

where the parameters and variables are defined in Appendix A.

The region radius of the front and rear edges of water flooding as a function of time can be obtained by solving the above equations simultaneously:

$$R_{I-II} = \sqrt{\frac{\pi h\varphi}{qBt}V_{CO_2,I-II}},\ R_{II-III} = \sqrt{\frac{\pi h\varphi}{qBt}V_{CO_2,II-III}} \tag{4}$$

where the parameters and variables are defined in Appendix A.

The model presented here does not account for the diffusion of water in gas. The quantity concentration of the CO_2 material at the right end face of zone I is equal to that at the left end face of zone II, and therefore, $D_{I-II} = 1$. Additionally, the impact of bound water is neglected; only movable gas exists in zone I and $f_g = 1$. Consequently, the speed of the front and rear edge movement before and after gas displacement by water can be determined using graphical methods. In Figure 3, the slope of line ① characterizes the moving speed of the leading edge, and the slope of line ② characterizes the moving speed of the trailing edge.

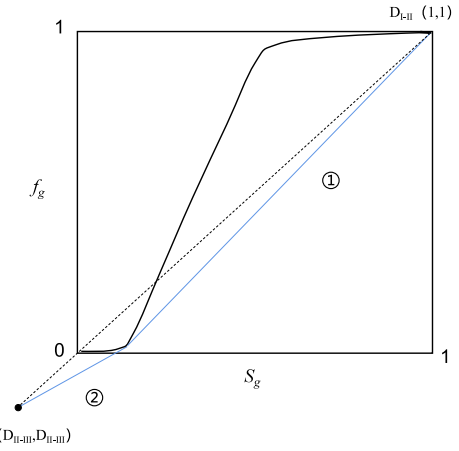

Figure 3. Water drive gas partial flow curve.

2.3. Mathematical Model for Multilayered Three-Zone Gas Reservoirs. A mathematical model for a three-layer, three-zone gas reservoir can be established based on the partial differential equation of seepage, along with initial, internal, external, and connectivity boundary conditions. This model assumes that a gas production well with a fixed flow rate is located at the center of a circular geological formation from the jth layer and kth zone:

https://doi.org/10.1021/acsomega.3c08949
ACS Omega 2024, 9, 12850−12865

$$\begin{cases} \dfrac{\partial^2 P_{j,k,D}}{\partial r_D^{\,2}} + \dfrac{1}{r_D}\dfrac{\partial P_{j,k,D}}{\partial r_D} = \dfrac{\omega_{j,k}}{e^{2S_1}\chi_{j,k}}\dfrac{\partial P_{j,k,D}}{\partial t_D}(j = 1, 2, 3; k = 1, 2, 3) \\ P_{j,1D}|_{t=0} = P_{j,2D}|_{t=0} = P_{j,3D}|_{t=0} = P_{ijD}(j = 1, 2, 3) \\ -\chi_{j,1}e^{S_1 - S_j}\dfrac{\partial P_{j,1D}}{\partial r_D} = q_{jD}(j = 1, 2, 3) \\ \sum_{j=1}^{3} q_{jD} = 1 \\ P_{j,1D}|_{r_D = r_{wejD}} = P_{wD}(j = 1, 2, 3) \\ P_{j,1D}|_{r_D = r_{j,1D}} = P_{j,2D}|_{r_D = r_{j,1}D}(j = 1, 2, 3) \\ \left.\dfrac{\partial P_{j,1D}}{\partial r_D}\right|_{r_D = r_{j,1D}} = M_{j,21}\left.\dfrac{\partial P_{j,2D}}{\partial r_D}\right|_{r_D = r_{j,2D}}(j = 1, 2, 3) \\ P_{j,2D}|_{r_D = r_{j,2D}} = P_{j,3D}|_{r_D = r_{j,2D}}(j = 1, 2, 3) \\ \left.\dfrac{\partial P_{j,2D}}{\partial r_D}\right|_{r_D = r_{j,2D}} = M_{j,32}\left.\dfrac{\partial P_{j,3D}}{\partial r_D}\right|_{r_D} = r_{j,2D}(j = 1, 2, 3) \\ P_{j,3D}|_{r = r_{cD}} = P_{ijD}(j = 1, 2, 3) \end{cases} \tag{5}$$

where the dimensionless parameters and variables are defined in Appendix B.

3. SOLUTION OF THE MODEL

3.1. Solution of the Corrected B−L Equation. The key to solving the equation lies in determining the solubility of CO_2 under certain temperature and pressure conditions. Numerous scholars have conducted extensive research on this dissolution problem.[10−12] For the sake of simplifying model calculations and facilitating application, this article adopts the empirical fitting formula proposed by Chang et al.[10] When $P < P^0$, the solubility of CO_2 in water is

$$R_{sw} = 14.5\theta P\left[1 - \beta\sin\left(\frac{\pi}{2}\frac{14.5\varepsilon P}{14.5\varepsilon P + 1}\right)\right] \tag{6}$$

When $P \geq P^0$, the solubility of CO_2 in water is

$$R_{sw} = \theta P^0(1 - \beta^3) + \chi(14.5P - P^0) \tag{7}$$

$$\begin{cases} \theta = \sum_{i=0}^{4}(\theta_i 10^{-3i} TF^i) \\ \beta = \sum_{i=0}^{4}(\beta_i 10^{-3i} TF^i) \\ \varepsilon = 10^{-3}\sum_{i=0}^{4}(\varepsilon_i 10^{-3i} TP^i) \\ P^0 = 0.04309\dfrac{\sin^{-1}(\beta^2)}{\varepsilon\left[1 - \frac{2}{\pi}\sin^{-1}(\beta^2)\right]} \\ \chi = \beta\left\{1 - \beta\left[\sin\left(\dfrac{\pi}{2}\dfrac{14.5\varepsilon P}{14.5\varepsilon P + 1}\right) + \dfrac{\pi}{2.5P^0 + 1}\cos\left(\dfrac{\pi}{2}\dfrac{\varepsilon P^0}{\varepsilon P^0 + 1}\right)\right]\right\} \\ TF = \dfrac{9}{5}(T - 273.15) + 32 \end{cases} \tag{8}$$

where the parameters and variables are defined in Appendix A.

The coefficients involved in the formula are shown in Table. 1. Through the above formula, the solubility of CO_2 in water under certain temperature and pressure conditions can be obtained. However, because the gas in the formation is not entirely CO_2, it also includes gases with weak solubility in water such as N_2. Therefore, it is necessary to consider the different content of CO_2 in the gas, and bring it into eq 2 to obtain the amount concentration of the substance converted into it. The graphical method can be used to obtain the movement speed of the front and rear edges of water drive gas and obtain the partition radius at different times, By introducing it into the following seepage mathematical model, the coupling of the B−L equation and the multilayer zonal mathematical model can be achieved.

Table 1. Coefficient Value of the Chang Model

	$i = 1$	$i = 2$	$i = 3$	$i = 4$	$i = 5$
θ	1.163	−16.630	111.073	−376.859	524.889
β	0.965	−0.272	0.0923	−0.1008	0.0998
ε	1.280	−10.757	52.696	−222.395	462.672

3.2. Solution of the Mathematical Model. The general solution of the equation containing the Bessel function is obtained by changing the dimensionless mathematical model through a pull function:

https://doi.org/10.1021/acsomega.3c08949
ACS Omega 2024, 9, 12850−12865

$$\begin{cases} \bar{P}_{sj,1D} = A_{j,1} I_0\left(\sqrt{\dfrac{\omega_{j,1}s}{e^{2S_1}\chi_{j,1}}}\, r_D\right) + B_{j,1} K_0\left(\sqrt{\dfrac{\omega_{j,1}s}{e^{2S_1}\chi_{j,1}}}\, r_D\right) + \dfrac{P_{ijD}}{s} \\ \bar{P}_{sj,2D} = A_{j,2} I_0\left(\sqrt{\dfrac{\omega_{j,2}s}{e^{2S_1}\chi_{j,2}}}\, r_D\right) + B_{j,2} K_0\left(\sqrt{\dfrac{\omega_{j,2}s}{e^{2S_1}\chi_{j,2}}}\, r_D\right) + \dfrac{P_{ijD}}{s} \\ \bar{P}_{sj,3D} = A_{j,3} I_0\left(\sqrt{\dfrac{\omega_{j,3}s}{e^{2S_1}\chi_{j,3}}}\, r_D\right) + B_{j,3} K_0\left(\sqrt{\dfrac{\omega_{j,3}s}{e^{2S_1}\chi_{j,3}}}\, r_D\right) + \dfrac{P_{ijD}}{s} \end{cases} \tag{9}$$

where the dimensionless parameters and variables are defined in Appendix B.

In the formula, $A_{j,1}$, $B_{j,1}$, $A_{j,2}$, $B_{j,2}$, $A_{j,3}$, and $B_{j,3}$ are undetermined coefficients. A six-element system of linear equations can be established by bringing in boundary and initial conditions. There are six unknowns in total. The solution can obtain $A_{j,1}$ and $B_{j,1}$ and then be brought in to obtain the bottom hole pressure solution $\overline{P_{swjD}}$. The expression of $A_{j,1}$ and $B_{j,1}$ is shown in Appendix C.

$$\overline{P_{swjD}} = A_{j,1} I_0\left(\sqrt{\frac{\omega_{j,1}s}{e^{2S_1}\chi_{j,1}}}\, r_{wejD}\right) + B_{j,1} K_0\left(\sqrt{\frac{\omega_{j,1}s}{e^{2S_1}\chi_{j,1}}}\, r_{wejD}\right) + \frac{P_{ijD}}{s} \tag{10}$$

The layered production contribution formula is then obtained based on Duhamel's principle:

$$q_{jD} = \frac{\left(s \times \dfrac{\sum_{j=1}^{3}\left(\frac{P_{ijD}}{s^2 \times P_{swjD} - s \times P_{ijD}} + \frac{1}{s}\right)}{\sum_{j=1}^{3}\left(\frac{1}{s \times P_{swjD} - P_{ijD}}\right)} - P_{ijD}\right)}{s^2 \times \bar{P}_{swjD} - s \times P_{ijD}} \tag{11}$$

When solving layered production q_{jD}, because of the need to solve the dynamic boundary $r_{j,1}$ and $r_{j,2}$ and involve the initial setting of layered production, it has been found through a large number of experiments and model derivation studies by predecessors that for multilayer gas reservoirs, regardless of whether the outer boundary is closed or constant pressure, at the initial stage of production, its production contribution is mainly defined according to the flow coefficient ratio given in this article. Therefore, when writing a program to solve the problem, it is only necessary to assign the flow coefficient ratio at the first time step. After that, the layered output of the time step will be calculated to achieve the solution of the layered output. Then, using the Stehfest numerical inversion method, the layered output of the real space can be obtained.

4. RESULT AND DISCUSSION

4.1. Model Validation. To verify the correctness of the above model and the accuracy of production splitting, it is assumed that there are only CO_2 and CH_4 in the formation. We comapared the model with the CMG numerical simulation results. See Figure 4 for the comparison diagram of the model results and Table 2 for the model parameters.

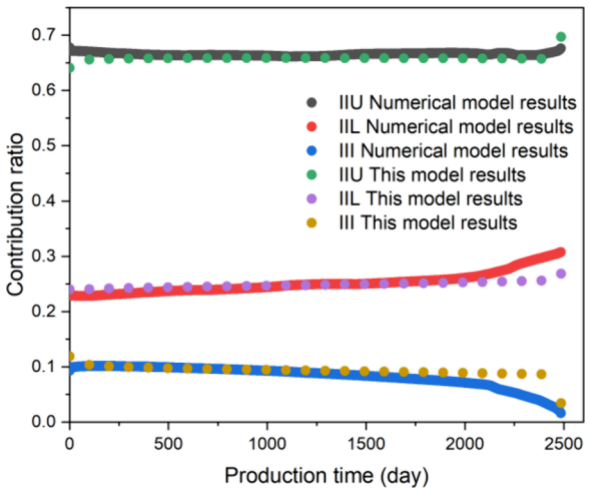

Figure 4. Comparison chart of yield splitting results.

Table 2. Digital Analog Validation Parameters

	first layer	second layer	third layer
thickness	9 m	6 m	3 m
permeability	0.01 D	0.005 D	0.005 D
porosity	0.3	0.2	0.1
gas viscosity	0.01517 mPa·s	0.0139 mPa·s	0.0136 mPa·s
water viscosity	0.373 mPa·s	0.373 mPa·s	0.373 mPa·s
gas compressibility factor	0.0198 1/MPa	0.0258 1/MPa	0.0351 1/MPa
water compressibility factor	0.00044 1/MPa	0.00044 1/MPa	0.00044 1/MPa
gas compressibility factor	0.000481 1/MPa	0.000481 1/MPa	0.000481 1/MPa
outer boundary distance	1000 m	1000 m	1000 m
CO_2 content	70%	50%	30%
well diameter	15.24 cm		
total gas production	200,000 m^3/d		

It can be seen that the established mathematical model can well deal with the production splitting problem of multilayer water drive gas reservoirs, the correctness and accuracy of the model have been verified, and the model can also well predict water breakthrough time. The main error of the model is that the output contribution of the aquifer will fluctuate sharply before water breakthrough. In the numerical model, the output contribution of the aquifer will gradually decrease to 0, but when the water breakthrough phenomenon is reflected in the model, the output contribution curve starts to diverge. Although there is a small error in comparing the prewater breakthrough model with the numerical simulation results, the consideration of CO_2 dissolution and inconsistent advancing speeds at the front and rear edges of water drive enriches the original production splitting theory of water drive gas reservoirs, making the assumptions and solutions of the mathematical model more consistent with actual gas reservoir conditions.

The accuracy of the model is verified again through actual gas field production performance. Taking a gas well in the South China Sea as an example, the well was vertically drilled through three formations without crossflow between the formations. The

https://doi.org/10.1021/acsomega.3c08949
ACS Omega 2024, 9, 12850−12865

input static physical properties parameters of the formation and the production parameters of the gas well are shown in Table 3.

Table 3. Parameter Table of a Gas Well in the South China Sea

	first layer	second layer	third layer
thickness	7.3 m	19.7 m	5 m
permeability	0.0051 D	0.1504 D	0.0714 D
porosity	0.1914	0.2959	0.2695
gas viscosity	0.0155 mPa·s	0.0155 mPa·s	0.0155 mPa·s
water viscosity	0.3443 mPa·s	0.3443 mPa·s	0.3443 mPa·s
gas compressibility factor	0.0934 1/MPa	0.0934 1/MPa	0.0853 1/MPa
water compressibility factor	0.00044 1/MPa	0.00044 1/MPa	0.00044 1/MPa
gas compressibility factor	0.000481 1/MPa	0.000481 1/MPa	0.000481 1/MPa
outer boundary distance	1504 m	1504 m	486 m
CO_2 content	65%	65%	72%
well diameter	15.24 cm		
total gas production	200,000 m^3/d		

After the well was put into production, production logging was conducted in the first, third, and sixth years. Because of the close spatial distance between the first and second layers of the well, it is difficult for production logging to split and interpret the gas production in the two layers. To avoid subjective conclusions, the first and second layers are treated as a whole. Comparing the model results with the production logging results, it can be found that this model can well reflect the gas production situation of each layer, and the error between the model prediction and the actual production logging does not exceed 10%. The third layer of the model experienced a decrease in the proportion of gas production during the production process due to the short outer boundary distance of the third layer. During the water drive gas process, because of the viscosity of water being greater than the gas viscosity, the flow capacity of the water zone was greater than that of the gas water transition zone. Because of the faster water advance speed of the third layer than that of the first and second layers, the proportion of contribution of the third layer showed a downward trend.

Comparing the simulation results of this well number, it can be found that the water breakthrough time predicted by the mathematical model is basically consistent with the theoretical model, which indicates that this model can not only achieve dynamic splitting of the production of multilayer combined production gas reservoirs but also achieve accurate prediction of the water breakthrough time of single layer water drive gas reservoirs. Based on this model, preliminary calculation of the dynamic reserves of small layers is conducted to provide data support for subsequent gas reservoir potential exploration. The model prediction results, numerical simulation results, and production logging results in this article are shown in Figure 5, and the comparison of the results and data is shown in Table 4.

Verified by the mechanism model and actual data, the model established in this paper can well reflect the formation supply capacity before water breakthrough and can accurately predict the water breakthrough time of each layer. During actual production, this method can be used to establish corresponding models in combination with PVT data measured in early production, well testing, logging, and other data to guide the production allocation of gas wells before water breakthrough so that each small layer can be fully utilized while controlling the edge water advancing speed of each layer, delaying the abandonment time of gas wells, and achieving the goal of improving oil recovery.

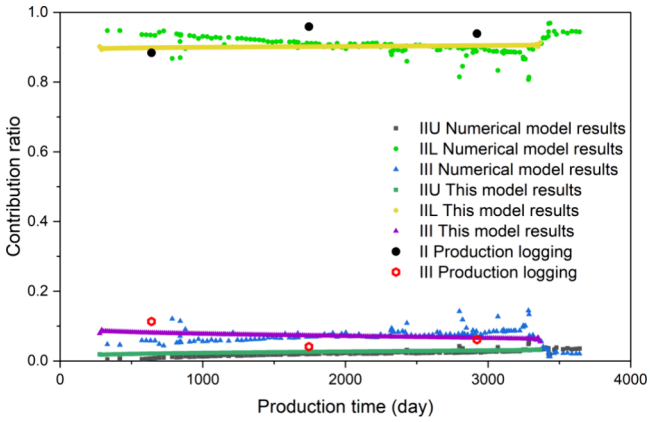

Figure 5. Model instance verification diagram.

Table 4. Comparison Table of Model, Digital Simulation, and Production Logging Results

		first layer + second layer	third layer
first year	results of this model	88.94%	11.06%
	logging results	88.30%	11.70%
	numerical simulation results	94.29%	5.71%
fourth year	results of this model	91.25%	8.75%
	logging results	95.90%	4.40%
	numerical simulation results	94.06%	5.94%
seventh year	results of this model	93.58%	6.42%
	logging results	93.90%	6.10%
	numerical simulation results	92.03%	7.97%

4.2. Sensitivity Analysis. The previous section confirmed the applicability of this model to actual formations. This section will conduct a sensitivity analysis of the model, taking into account the quantitative relationship between the six parameters of permeability, outer boundary distance, porosity, thickness, different CO_2 content, and total gas production rate and the change in gas production contribution. The parameters used for model verification are shown in Table 5.

Table 5. Basic Parameters for Model Sensitivity Analysis

	first layer	second layer	third layer
thickness	10 m	10 m	10 m
permeability	0.1 D	0.1 D	0.1 D
porosity	0.2	0.2	0.2
gas viscosity	0.0155 mPa·s	0.0155 mPa·s	0.0155 mPa·s
water viscosity	0.3443 mPa·s	0.3443 mPa·s	0.3443 mPa·s
gas compressibility factor	0.0934 1/MPa	0.0934 1/MPa	0.0934 1/MPa
water compressibility factor	0.00044 1/MPa	0.00044 1/MPa	0.00044 1/MPa
gas compressibility factor	0.000481 1/MPa	0.000481 1/MPa	0.000481 1/MPa
outer boundary distance	1000 m	1000 m	1000 m
CO_2 content	65%	65%	65%
well diameter	15.24 cm		
total gas production	200,000 m^3/d		

https://doi.org/10.1021/acsomega.3c08949
ACS Omega 2024, 9, 12850−12865

We defined the production time before layered water breakthrough as the anhydrous recovery period; selected 25, 50, and 75% of the anhydrous recovery period as the pre, mid, and late gas production time nodes; and analyzed the change rule of the contribution ratio of the layered production period at the above time nodes.

4.2.1. Permeability. The permeability of the first layer of the given model is 100, 200, 300, 400, and 600 mD, respectively. The remaining parameters remain unchanged and are brought into the model in this paper. See Figure 6 for the variation rule of

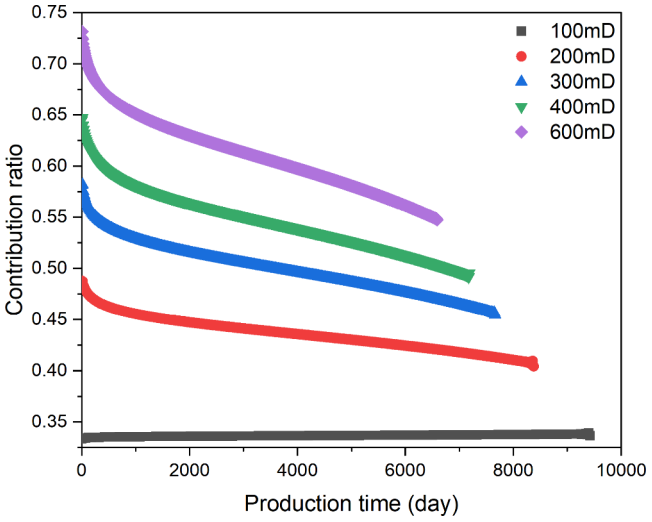

Figure 6. Comparison of the production contribution of different permeability.

the contribution ratio of gas production with different permeability Figure 7 for the variation rule of the contribution

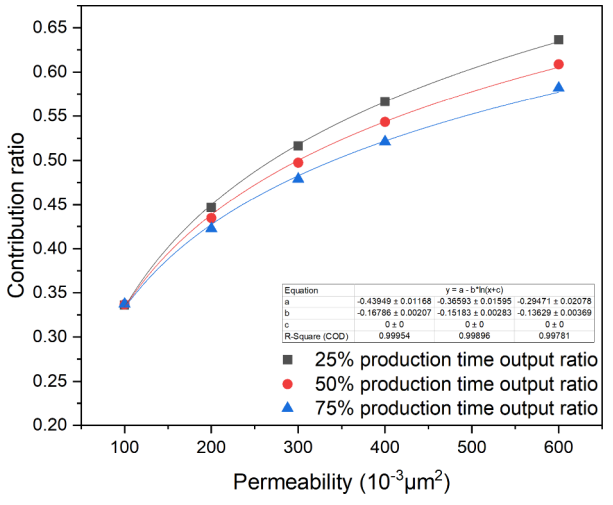

Figure 7. Variation law of contribution of different permeability layers at different times.

of different permeability layers at different times, and Figure 8 for the variation rule of water breakthrough time with permeability. It can be seen that as the permeability of the first layer increases, the initial gas production contribution of the first layer continues to increase. When the permeability of the first layer is higher than that of other layers, the contribution of the first layer to gas production decreases with the increase of

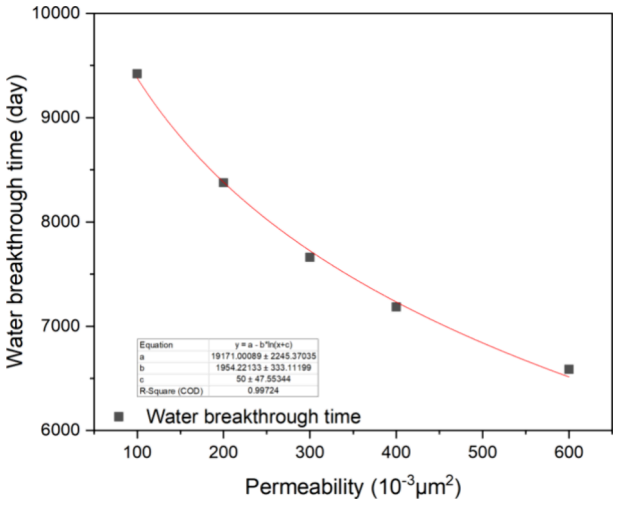

Figure 8. Variation pattern of water breakthrough time with permeability.

production time. When the parameters of each layer are consistent, the contribution ratio of layered gas production is consistent, and the production of multilayer gas reservoirs can be considered as the production of single layer gas reservoirs. Comparing the coefficients of the gas production contribution curve of the first layer at different times, it can be found that the higher the permeability of the first layer is, the faster the gas production contribution decreases as the gas production time increases, the greater is the difference between the pre, mid, and late gas production contributions, and the shorter is the anhydrous recovery period. The change in gas production contribution ratio of the first layer is logarithmic to the change in permeability and the change in anhydrous recovery period.

4.2.2. Outer Boundary Distance. Given that the outer boundary distances of the first layer of the model are 500, 625, 750, 875, 1000, 1250, and 1500 m, the remaining parameters remain unchanged. Taking into account the model established above, the variation rule of the gas production contribution ratio for different outer boundary distances is shown in Figure 9. It can be seen that as the outer boundary distance of the first layer

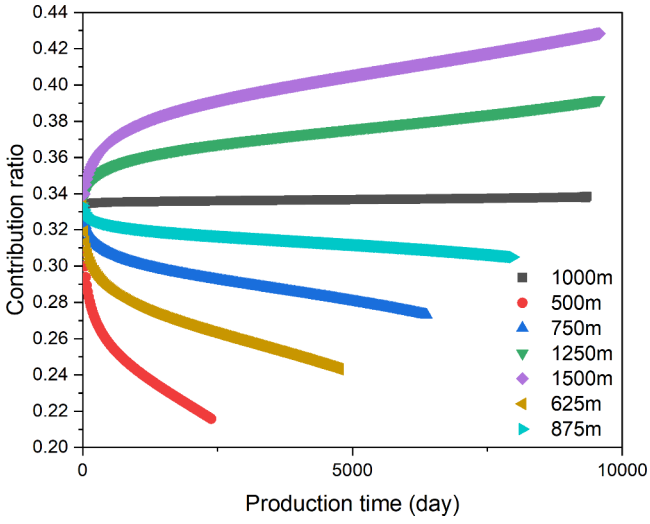

Figure 9. Comparison of the output contribution of different outer boundary distances.

https://doi.org/10.1021/acsomega.3c08949
ACS Omega 2024, 9, 12850−12865

increases, the gas production contribution of the first layer continues to increase. When the outer boundary distance of the first layer is smaller than that of other layers, the gas production contribution ratio of the first layer presents a downward trend with the increase of production time. When the outer boundary distance of the first layer is larger than that of other layers, the gas production contribution ratio of the first layer presents an upward trend with the increase in production time.

See Figure 10 for the variation rule of layered contribution at different times and different outer boundary distances and

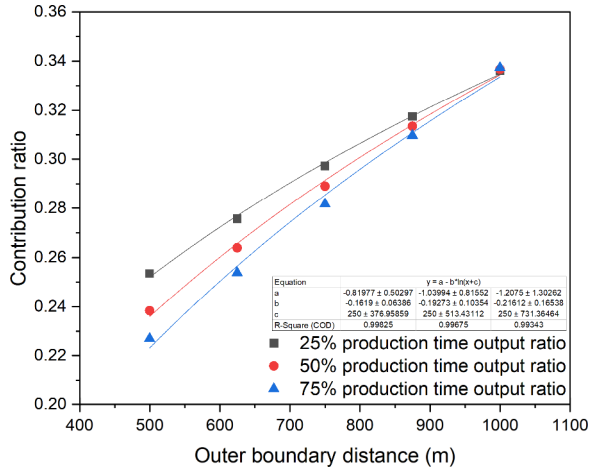

Figure 10. Variation law of layered contribution of different outer boundary distances at different times.

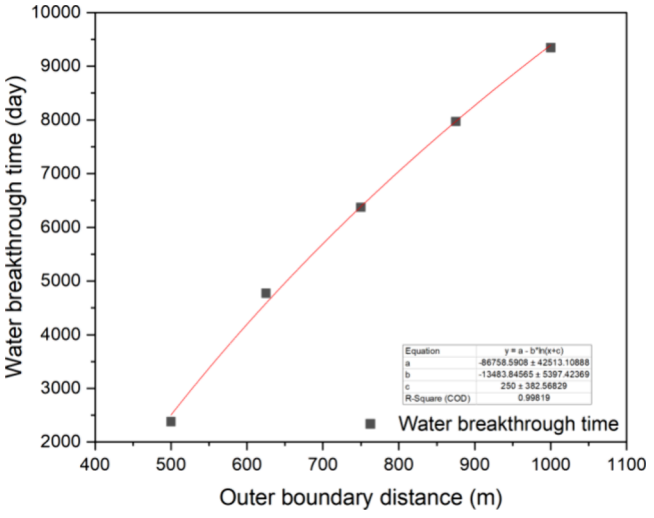

Figure 11. Variation pattern of water breakthrough time with outer boundary distance.

Figure 11 for the variation rule of water exposure time with outer boundary distances. Comparing the gas production contribution curve of the first layer at different times, it can be found that compared to the early stage of anhydrous recovery, the gas production contribution of each layer in the later stage is more affected by the outer boundary distance. The greater the difference in the outer boundary distance of each layer is, the greater is the difference in its gas production contribution before, during, and after the formation. The smaller the outer boundary distance of this layer is, the shorter is the anhydrous recovery period. The contribution ratio of gas production in the first layer is in a power relationship with the change of outer boundary distance, and the water-free recovery period in the first layer is in a logarithmic relationship with the change of outer boundary distance.

4.2.3. Porosity. The porosities of the first layer of a given model are 10, 15, 20, 25, and 30%. The remaining parameters remain unchanged, and the model established above is brought in. The variation rule of the gas production contribution ratio of different porosity is shown in Figure 12, the variation rule of the

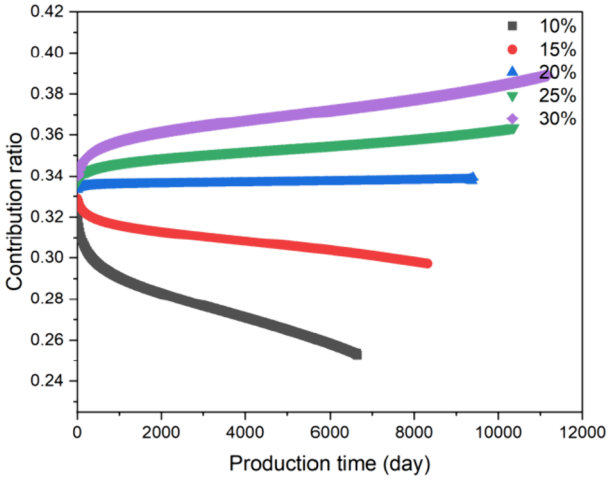

Figure 12. Variation pattern of contribution of different porosity layers.

contribution of different porosity layers at different times is shown in Figure 13, and the variation rule of water exposure time

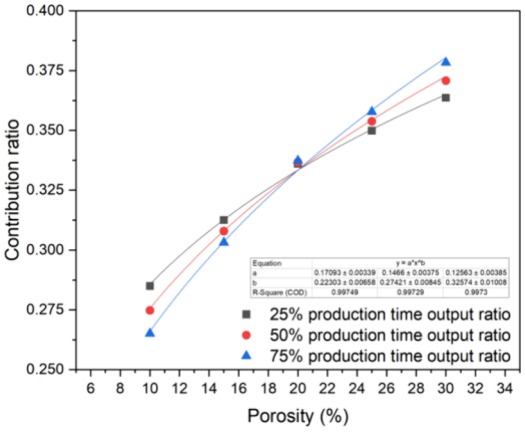

Figure 13. Variation pattern of contribution of different porosity layers at different times.

with porosity is shown in Figure 14. It can be seen that as the porosity of the first layer increases, the contribution of the first layer to gas production continues to increase. When the porosity of the first layer is smaller than that of other layers, the gas production contribution ratio of the first layer presents a downward trend with the increase of production time. When the porosity of the first layer is larger than that of other layers, the gas production contribution ratio of the first layer presents an upward trend with the increase of production time; The smaller the porosity of this layer is, the shorter is the anhydrous recovery period, and there is a logarithmic relationship between the

https://doi.org/10.1021/acsomega.3c08949
ACS Omega 2024, 9, 12850−12865

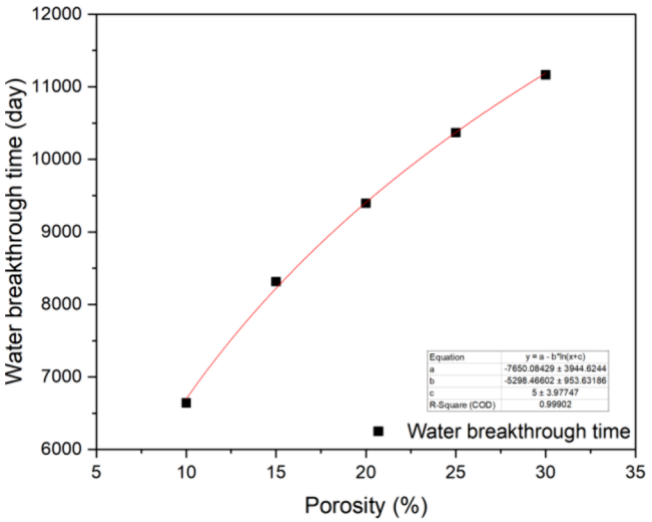

Figure 14. Variation pattern of water breakthrough time with porosity.

anhydrous recovery period and the porosity change; The contribution ratio of gas production in the first layer is exponentially related to the porosity change.

4.2.4. Thickness. The thickness of the first layer of the given model is 5, 7 5, 10, 12.5, and 15 m, and the remaining parameters remain unchanged. Taking into account the model established above, the variation rule of gas production contribution ratio for different thicknesses is shown in Figure 15. It can be seen that as

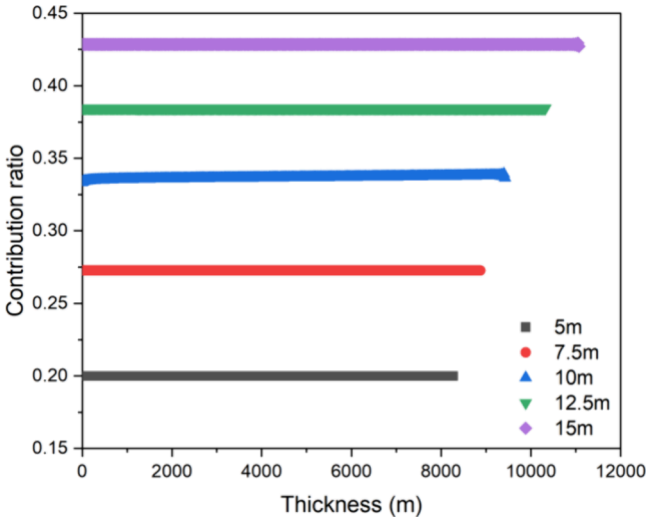

Figure 15. Variation of contribution of different thickness layers.

the thickness of the first layer increases, the contribution of the first layer to gas production continues to increase; As thickness is a dimensionless auxiliary parameter involved in the definition of flow coefficient and reservoir capacity coefficient, when the thickness of each layer increases or decreases, the contribution of each layer to gas production remains stable in the early, middle, and late stages.

See Figure 16 for the variation rule of contribution of different layers with different thicknesses at different times and Figure 17 for the variation rule of water exposure time with thickness. The smaller the thickness of this layer is, the shorter the anhydrous recovery period. The anhydrous recovery period of the first layer has a logarithmic relationship with the thickness change. The

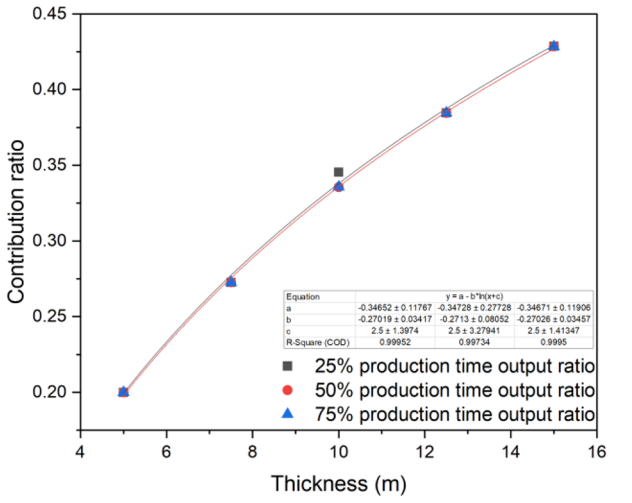

Figure 16. Variation law of contribution of different thickness layers at different times.

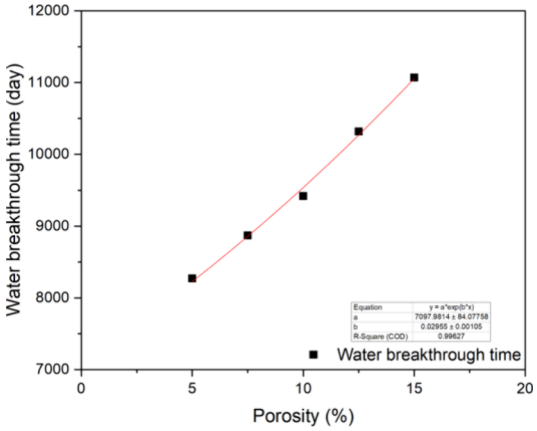

Figure 17. Variation pattern of water breakthrough time with thickness.

contribution ratio of the first layer to production has a logarithmic relationship with the thickness change.

4.2.5. CO_2 Content. Given that the CO_2 content of the first layer of the model is 5, 25, 45, 65, and 85%, the remaining parameters remain unchanged and are brought into the model in this article. The CO_2 content is a parameter that needs special consideration in this model. First, changes in the CO_2 content directly affect the viscosity of the gas under the same temperature and pressure conditions. For underground conditions of 13 MPa and 80 °C, the gas viscosity first decreases and then increases with the CO_2 content. As shown in Figure 18, when the CO_2 content is 35%, the gas viscosity reaches the lowest value of 0.01355 mPa·s. The nonmonotonic change in viscosity makes the variation trend of fluid fluidity in the formation with CO_2 content different (the variation trend of multilayer and multi zone flow coefficient is different), which makes the contribution of early gas production higher when the CO_2 content in Figure 19 is 25 and 45% and the contribution of gas production lowest when the CO_2 content is 85%. Second, the difference in CO_2 content makes the amount and concentration of CO_2 dissolved in water different. According to eq 2, as the CO_2 content increases, the advancing speed of the water drive trailing edge gradually increases, the water zone scope expands faster, and the seepage resistance of this layer will be greater. However, according to Section 4.1, the contribution

https://doi.org/10.1021/acsomega.3c08949
ACS Omega 2024, 9, 12850−12865

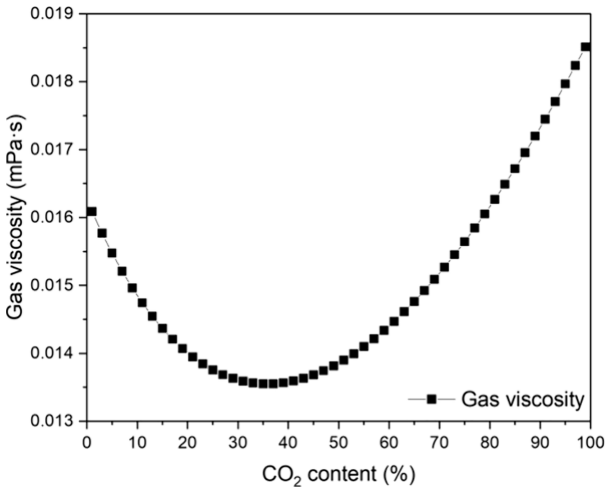

Figure 18. Variation of gas viscosity with the CO_2 content.

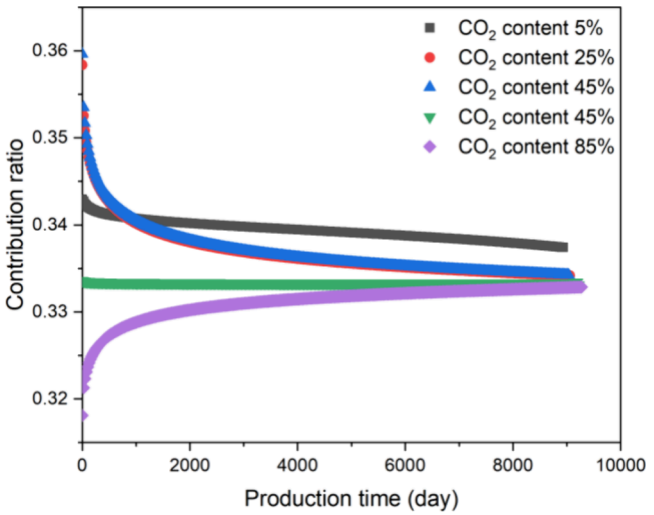

Figure 19. Variation pattern of layered contribution of different CO_2 contents.

of gas production from formations with different permeabilities (flow coefficients) tends to converge after a period of production; therefore, there is no obvious phenomenon that the gas production contribution curve and water breakthrough time curve change with the CO_2 content in the figure.

Although it is difficult to quantitatively evaluate the contribution law of gas production because of the influence of gas viscosity and water drive speed, the CO_2 content is still a parameter that cannot be ignored in the model. In the early stage of edge water invasion, the difference in the CO_2 content of the first layer will cause a deviation in the contribution ratio of gas production of more than 4%, which will greatly affect the prediction of the water breakthrough time in each layer at the end of production and the formulation of production allocation systems for each layer during the entire production cycle.

4.2.6. Total Gas Production Rate. When the physical property parameters of each layer are consistent, the change in the total gas production rate has almost no impact on the gas production contribution of each layer. However, when the physical properties, especially the permeability, of each layer are different, the change in the total gas production rate has a significant impact on the contribution of each layer to gas production.

Given that the permeability of the three layers is 200, 100, and 50 mD, respectively, and the total gas production rate is 100,000, 200,000, 400,000, and 600,000 m^3, respectively, the remaining parameters remain unchanged, and the model established above is taken into account. The change rule of gas production contribution ratio for different total gas production rates is shown in Figure 20, the change rule of layered contribution for

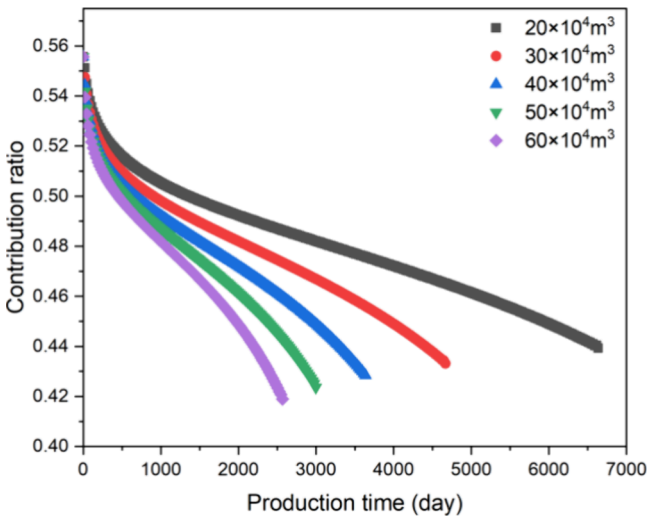

Figure 20. Variation of the contribution of high permeability layers with different total production.

different total gas production rates at different times is shown in Figure 21, and the change rule of water breakthrough time with

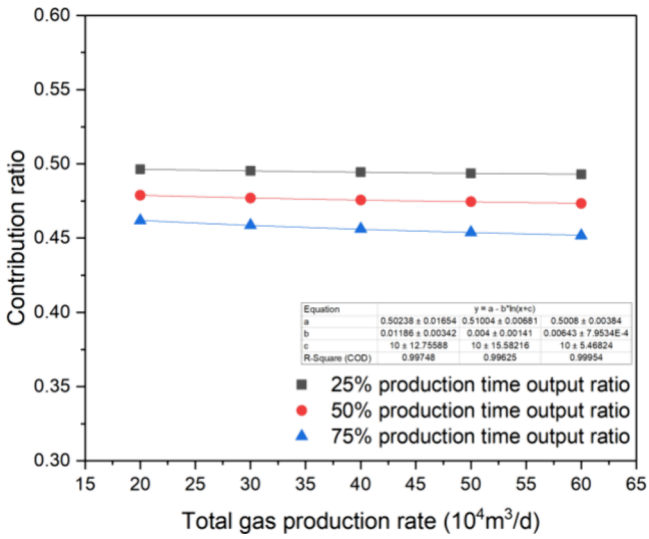

Figure 21. Variation law of the production of a high permeability layer with different total production at different times.

total gas production rate is shown in Figure 22. It can be seen that the contribution of the first layer of gas production has a downward trend. For this model, increasing the total gas production speed is equivalent to increasing the water drive speed, accelerating the expansion of the same layer of the water zone, and increasing the single layer seepage resistance. Therefore, changes in the total gas production speed will have an impact on the contribution of the layered gas production, and as the total gas production speed increases, the decline rate of

https://doi.org/10.1021/acsomega.3c08949
ACS Omega 2024, 9, 12850−12865

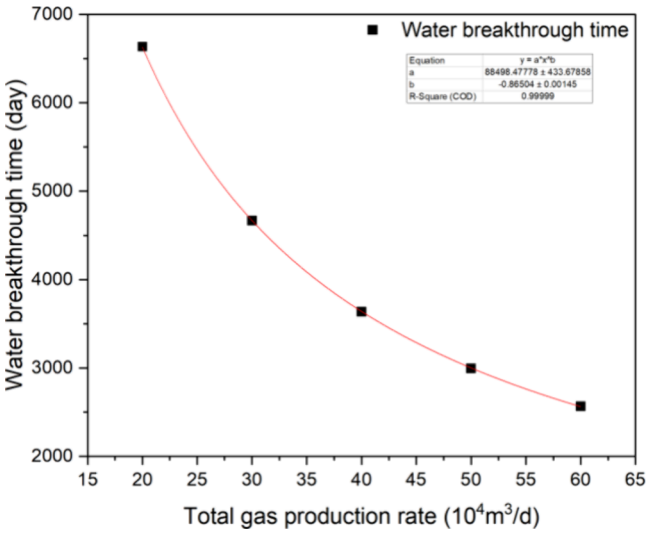

Figure 22. Variation pattern of water breakthrough time with total gas production rates.

the first layer of gas production contribution continues to increase. The higher the total gas production rate, the greater the difference between the gas production contribution of each layer in the production process, and the shorter the anhydrous recovery period; the proportion of the gas production contribution of the first layer has an exponential relationship with the change of the total gas production rate, and the first anhydrous recovery period has a multiplicative power relationship with the change of the total gas production rate.

4.3. Rank of Main Control Factors for Gas Production Contribution at the Reservoir Scale. *4.3.1. Orthogonal Experimental Scheme.* Based on the results of the single-factor sensitivity analysis of the above gas production contribution parameters, using the contribution ratio of layered gas production as an evaluation index, six factors are selected, including permeability, outer boundary distance, porosity, thickness, CO_2 content, and total gas production speed. Each factor is designed with three levels. The factor level table is shown in Table 6.

Because of the fact that this experiment is based on six factors and three levels, orthogonal table L_{18} was selected for the orthogonal experimental scheme design, and a total of 18 groups of experiments were conducted. The specific experimental scheme and physical property data of the other two layers are shown in Table 7.

4.3.2. Analysis of Orthogonal Experimental Results. Multivariate variance analysis was used to study the difference relationship between the contribution of six factors, namely, permeability, outer boundary distance, thickness, porosity, CO_2 content, and total gas production rate, to the early, middle, and late stage of the gas production. The contribution results of gas production from each layer are shown in Table 8. The results are shown in Table 9. The six parameters can explain 98.0% of the changes in the proportion of early gas production, 98.7% of the changes in the proportion of midterm gas production, and 97.4% of the changes in the proportion of late gas production.

In terms of reservoir scale, in the early stage of parallel water drive gas, the order of influence degree of each parameter on layered gas production is permeability > thickness > outer boundary distance > porosity > CO_2 content > total gas production speed. In the middle and late stages of parallel water drive gas, the order of influence degree of each parameter on layered gas production is thickness > permeability > outer boundary distance > porosity > CO_2 content > total gas production speed. Layered thickness is widely involved in the definition of dimensionless variables in this model. At this time, thickness not only affects the layered reservoir capacity ratio but also affects the layered flow coefficient ratio. Therefore, thickness will become the most dominant factor in the later stage. The contribution ratio of layered gas production gradually decreases with time, whereas the impact of porosity and outer boundary distance gradually increases. That is, the impact of reserves on the contribution of layered gas production gradually increases, but it is not sufficient to change the dominant position of the flow coefficient corresponding to permeability and thickness in the contribution of layered gas production.

5. SUMMARY AND CONCLUSIONS

In this paper, the B−L equation considering gas dissolution is first established to derive the moving velocity of the leading and trailing edges of water-driven gas replacement in high-CO_2 gas reservoirs, and it is introduced into the multilayer water-driven gas seepage model without interlayer scuttling. It is demonstrated that the model can be well applied to production splitting of multilayer water-driven high-CO_2 gas reservoirs through the solving and validation of the model. Compared with the traditional KH method, the model in this paper reflects the dynamic change of the supply of each layer in the process of multilayer water-driven gas; compared with the direct production logging or geochemical testing methods, the model in this paper can be based on the fluid properties and geologic parameters to measure the percentage of the contribution of each layer to the gas production, which has inexpensive and time-saving advantages. The specific conclusions are as follows:

1. A multilayer water-driven gas reservoir production splitting model without interlayer flow considering CO_2 dissolution is established, based on which the multilayer water-driven gas reservoir production splitting model is applied to the mechanistic model and a multilayer water-driven gas well in Nanhai, respectively, and the model is able to predict the time of seeing water in the layers wells wells wells, and the model in this paper predicts that the gas production contribution of each layer has an error of no more than 10% with the numerical simulation model results and the production logging results of a multi-layer combined well in the South China Sea.
2. CO_2 content is proposed as an important parameter to improve the accuracy of multilayer parallel water-driven

Table 6. Orthogonal Experiment Level Factor Table

level	permeability (μm^2)	outer boundary distance (m)	porosity (%)	thickness (m)	CO_2 content (%)	total gas production ($\times 10^4$ m^3)
1	100	500	15	5	5	20
2	300	1000	20	10	45	30
3	500	1500	25	15	85	40

https://doi.org/10.1021/acsomega.3c08949
ACS Omega 2024, 9, 12850−12865

Table 7. Orthogonal Experiment Plan Table

number	permeability (μm^2)	outer boundary distance (m)	porosity (%)	thickness (m)	CO_2 content (%)	total gas production ($\times 10^4$ m^3)
1	100	500	15	5	5	20
2	100	500	20	10	85	40
3	100	1000	25	5	85	30
4	100	1000	15	15	45	40
5	100	1500	25	10	45	20
6	100	1500	20	15	5	30
7	300	500	25	5	45	40
8	300	500	15	15	85	30
9	300	1000	20	10	45	30
10	300	1000	25	15	5	20
11	300	1500	20	5	85	20
12	300	1500	15	10	5	40
13	500	500	25	10	5	30
14	500	500	20	15	45	20
15	500	1000	20	5	5	40
16	500	1000	15	10	85	20
17	500	1500	15	5	45	30
18	500	1500	25	15	85	40
another two stratigraphic data	100	1500	25	15	45	

Table 8. Orthogonal Experiment Result Table

number	permeability (μm^2)	outer boundary distance (m)	porosity (%)	thickness (m)	CO_2 content (%)	total gas production ($\times 10^4$ m^3)	early-stage gas production contribution ratio (%)	medium-term gas production contribution ratio (%)	late-stage gas production contribution ratio (%)
1	100	500	15	5	5	20	7.85	6.21	5.29
2	100	500	20	10	85	40	14.92	12.15	10.39
3	100	1000	25	5	85	30	14.63	13.19	12.32
4	100	1000	15	15	45	40	26.45	23.55	21.51
5	100	1500	25	10	45	20	25.57	25.25	25.14
6	100	1500	20	15	5	30	31.95	31.41	30.92
7	300	500	25	5	45	40	13.92	10.79	8.98
8	300	500	15	15	85	30	37.06	29.21	24.40
9	300	1000	20	10	45	30	34.86	30.19	27.00
10	300	1000	25	15	5	20	47.90	43.11	39.54
11	300	1500	20	5	85	20	25.60	23.35	21.63
12	300	1500	15	10	5	40	39.30	35.47	32.49
13	500	500	25	10	5	30	40.28	32.15	26.95
14	500	500	20	15	45	20	49.00	40.21	35.08
15	500	1000	20	5	5	40	29.78	24.78	21.55
16	500	1000	15	10	85	20	44.49	38.06	33.65
17	500	1500	15	5	45	30	30.91	26.73	24.02
18	500	1500	25	15	85	40	61.53	57.71	54.24

gas production splitting in high-carbon gas reservoirs. Using the production splitting model established in this paper, the influence of CO_2 content on gas production contribution is quantitatively analyzed, and the accuracy of the model considering the influence of gas CO_2 content can be improved by 4%.

The quantitative relationship between the gas production contribution of each layer and each main control factor during the full production cycle is clarified. In the early stage of parallel water-driven gas production, the order of influence of gas production contribution from each layer is permeability > thickness > outer boundary distance > porosity > CO_2 content > total gas production rate. With the increase of gas production time, the influence of permeability and thickness gradually decreases, and the influence of storage capacity gradually increases. In the late stage of parallel water-driven gas production, the order of influence of the layered gas production contribution is thickness > permeability > outer boundary distance > porosity > CO_2 content > total gas production rate, and permeability and thickness are always the most important factors affecting the proportion of the layered gas production contribution in parallel water-driven gas reservoirs.

The model in this paper cannot simulate the production contribution relationship after the gas wells see water; first, the demarcation of the gas−gas−water transition zone-water zone in the model is determined by the moving speed of the water-driven gas front and back edge. Once water is seen, it means that the speed of the water-driven front edge is zero, and the model is no longer convergent. Second, the model for the water saturation in the gas−water transition zone is approximated as the average water saturation of the gas−water Second, the model

https://doi.org/10.1021/acsomega.3c08949
ACS Omega 2024, 9, 12850−12865

Table 9. Analysis Table of Variance of Contribution Ratio of Stratified Gas Production in Different Periods of the Orthogonal Experiment

		quadratic sum	df	mean square	F	p
early stage	intercept	1.843	1	1.843	1542.166	0.000
	permeability	0.152	2	0.076	63.645	0.000
	outer boundary distance	0.023	2	0.012	9.761	0.019
	thickness	0.145	2	0.072	60.577	0.000
	porosity	0.003	2	0.002	1.463	0.316
	CO_2 content	0.003	2	0.002	1.339	0.342
	total gas production	0.002	2	0.001	0.791	0.503
	residual error	0.006	5	0.001		
	factor rank	permeability > thickness > outer boundary distance > porosity > CO_2 content > total gas production rate				
	$R^2 = 0.982$					
medium term	intercept	1.408	1	1.408	1106.130	0.000
	permeability	0.097	2	0.049	38.255	0.001
	outer boundary distance	0.041	2	0.020	15.916	0.007
	thickness	0.121	2	0.061	47.541	0.001
	porosity	0.005	2	0.003	2.050	0.224
	CO_2 content	0.003	2	0.002	1.215	0.372
	total gas production	0.002	2	0.001	0.693	0.542
	residual error	0.006	5	0.001		
	factor rank	thickness > permeability > outer boundary distance > porosity > CO_2 content > total gas production rate				
	$R^2 = 0.977$					
late stage	intercept	1.151	1	1.151	883.179	0.000
	permeability	0.068	2	0.034	25.918	0.002
	outer boundary distance	0.050	2	0.025	19.278	0.004
	thickness	0.105	2	0.052	40.191	0.001
	porosity	0.006	2	0.003	2.382	0.188
	CO_2 content	0.002	2	0.001	0.953	0.446
	total gas production	0.002	2	0.001	0.756	0.517
	residual error	0.007	5	0.001		
	factor rank	thickness > permeability > outer boundary distance > porosity > CO_2 content > total gas production rate				
	$R^2 = 0.974$					

approximates the water saturation in the gas−water transition zone as the average water saturation in the gas−water transition zone, and the relationship of water saturation in the transition zone changes after the model sees water, so the model is no longer accurate. However, we can judge the time of seeing water in a certain layer by the nonconvergence time of the model so as to predict the time of seeing water in gas wells and realize the calculation of water-free recovery rate of water-driven gas reservoirs.

APPENDIX B

Total reservoir thickness:

$$h_t = \sum_{j=1}^{3} h_j \tag{B1}$$

Thickness weighted interlayer average fluidity:

$$\left(\frac{K}{\mu}\right)_a = \frac{1}{h_t}\sum_{j=1}^{3}\left[\frac{K_{j,1}K_{rg,j,1}}{\mu_{g,j,1}} + \left(\frac{K_{j,2}K_{rg,j,2}}{\mu_{g,j,2}} + \frac{K_{j,2}K_{rw,j,2}}{\mu_{g,j,2}}\right)_{S_{g,ave}^{II}} + \frac{K_{j,3}K_{rw,j,3}}{\mu_{w,j,3}}\right]h_j \tag{B2}$$

Average reservoir capacity coefficient between layers weighted by thickness:

$$(\varphi C_t)_a = \frac{1}{h_t}\sum_{j=1}^{3}(\varphi_{j,1}C_{t,j,1} + \varphi_{j,2}C_{t,j,2} + \varphi_{j,3}C_{t,j,3})h_j \tag{B3}$$

Average interlayer conductivity coefficient:

$$\eta_a = \frac{(K/\mu)_a}{(\varphi C_t)_a} \tag{B4}$$

Flow coefficient ratio between layers in zone i of layer j:

$$\chi_{j,i} = \frac{(K_{j,i}K_{rg,j,i}/\mu_{g,j,i})h_j}{(K/\mu)_a h_t} \tag{B5}$$

https://doi.org/10.1021/acsomega.3c08949
ACS Omega 2024, 9, 12850−12865

$$\sum_{j=1}^{3}(\chi_{j,1}+\chi_{j,2}+\chi_{j,3})=1 \tag{B6}$$

Reservoir capacity ratio between layers in zone i of layer j:

$$\omega_{j,i}=\frac{(\varphi_{j,i}C_{t,j,i})h_j}{(\varphi C_t)_a} \tag{B7}$$

$$\sum_{j=1}^{3}(\omega_{j,1}+\omega_{j,2}+\omega_{j,3})=1 \tag{B8}$$

The mobility ratio of zone 2 to zone *1* in layer j:

$$M_{j,21}=\frac{(K_{j,2}K_{rg,j,2}/\mu_{g,j,2})h_j}{(K_{j,1}K_{rg,j,1}/\mu_{g,j,1})h_j} \tag{B9}$$

The mobility ratio of zone 3 to zone 2 in layer j:

$$M_{j,32}=\frac{(K_{j,3}K_{rg,j,3}/\mu_{g,j,3})h_j}{(K_{j,2}K_{rg,j,2}/\mu_{g,j,2})h_j} \tag{B10}$$

Dimensionless pressure in zone i of layer j:

$$P_{j,iD}=\frac{(K/\mu)_a h_t}{1.842\times10^{-3}qB}(P_r-P_{j,i}) \tag{B11}$$

Dimensionless time:

$$t_D=\frac{3.6\eta_a}{r_w^2}t \tag{B12}$$

Dimensionless production:

$$q_{jD}=\frac{q_jB_j}{qB} \tag{B13}$$

Dimensionless distance:

$$r_D=\frac{r}{r_we^{-S_1}} \tag{B14}$$

Dimensionless radius of zone i of layer j:

$$r_{j,iD}=\frac{r_{j,i}}{r_we^{-S_1}} \tag{B15}$$

The dimensionless outer boundary distance of layer j:

$$r_{ejD}=\frac{r_{ej}}{r_we^{-S_1}} \tag{B16}$$

Dimensionless effective well radius of layer j:

$$r_{wejD}=e^{S_1-S_j} \tag{B17}$$

Appendix C

Given that the undetermined coefficients involved a large number of Bessel function calculations, the parameters repeatedly involved were defined as follows:

$$\begin{cases}
A1=\sqrt{\dfrac{\omega_{j,1}s}{e^{2S_1}\chi_{j,1}}}I_1\left(\sqrt{\dfrac{\omega_{j,1}s}{e^{2S_1}\chi_{j,1}}}\right),\ B1=\sqrt{\dfrac{\omega_{j,1}s}{e^{2S_1}\chi_{j,1}}}K_1\left(\sqrt{\dfrac{\omega_{j,1}s}{e^{2S_1}\chi_{j,1}}}\right),\\
C1=-\dfrac{1}{e^{2S_1}\chi_{j,1}s},\ A2=I_0\left(\sqrt{\dfrac{\omega_{j,1}s}{e^{2S_1}\chi_{j,1}}}r_{j,1D}\right)\\
B2=K_0\left(\sqrt{\dfrac{\omega_{j,1}s}{e^{2S_1}\chi_{j,1}}}r_{j,1D}\right),\ A3=I_0\left(\sqrt{\dfrac{\omega_{j,2}s}{e^{2S_1}\chi_{j,2}}}r_{j,1D}\right)\\
B3=K_0\left(\sqrt{\dfrac{\omega_{j,2}s}{e^{2S_1}\chi_{j,2}}}r_{j,1D}\right),\ A4=I_0\left(\sqrt{\dfrac{\omega_{j,2}s}{e^{2S_1}\chi_{j,2}}}r_{j,2D}\right)\\
B5=K_0\left(\sqrt{\dfrac{\omega_{j,3}s}{e^{2S_1}\chi_{j,3}}}r_{j,2D}\right),\ A6=\sqrt{\dfrac{\omega_{j,1}s}{e^{2S_1}\chi_{j,1}}}I_0\left(\sqrt{\dfrac{\omega_{j,1}s}{e^{2S_1}\chi_{j,1}}}r_{j,1D}\right)\\
B6=\sqrt{\dfrac{\omega_{j,1}s}{e^{2S_1}\chi_{j,1}}}K_0\left(\sqrt{\dfrac{\omega_{j,1}s}{e^{2S_1}\chi_{j,1}}}r_{j,1}\right),\ A7=M_{j,21}\sqrt{\dfrac{\omega_{j,2}s}{e^{2S_1}\chi_{j,2}}}I_1\left(\sqrt{\dfrac{\omega_{j,2}s}{e^{2S_1}\chi_{j,2}}}r_{j,1D}\right)\\
B7=M_{j.21}\sqrt{\dfrac{\omega_{j,2}s}{e^{2S_1}\chi_{j,2}}}K_1\left(\sqrt{\dfrac{\omega_{j,2}s}{e^{2S_1}\chi_{j,2}}}r_{j,1D}\right),\ AB=\sqrt{\dfrac{\omega_{j,2}s}{e^{2S_1}\chi_{j,2}}}I_1\left(\sqrt{\dfrac{\omega_{j,2}s}{e^{2S_1}\chi_{j,2}}}r_{j,2D}\right)\\
B8=\sqrt{\dfrac{\omega_{j,2}s}{e^{2S_1}\chi_{j,2}}}K_1\left(\sqrt{\dfrac{\omega_{j,2}s}{e^{2S_1}\chi_{j,2}}}r_{j,2D}\right),\ A9=M_{j,32}\sqrt{\dfrac{\omega_{j,3}s}{e^{2S_1}\chi_{j,3}}}I_1\left(\sqrt{\dfrac{\omega_{j,3}s}{e^{2S_1}\chi_{j,3}}}r_{j,2D}\right)\\
B9=M_{j,32}\sqrt{\dfrac{\omega_{j,3}s}{e^{2S_1}\chi_{j,3}}}K_1\left(\sqrt{\dfrac{\omega_{j,3}s}{e^{2S_1}\chi_{j,3}}}r_{j,2D}\right),\ A10=I_0\left(\sqrt{\dfrac{\omega_{j,3}s}{e^{2S_1}\chi_{j,3}}}r_{e1D}\right)\\
B10=K_0\left(\sqrt{\dfrac{\omega_{j,3}s}{e^{2S_1}\chi_{j,3}}}r_{e1D}\right)
\end{cases} \tag{C1}$$

The final solution is as follows:

https://doi.org/10.1021/acsomega.3c08949
ACS Omega 2024, 9, 12850−12865

$$A_{j,1} = \{C1^*[(-B6^*A3^*B2^*A7)^*(-A5^*B10^*B8 + A10^*B8^*B5 - B4^*A9^*B10^*B7^*B9^*A10) + (-B6^*B3 + B2^*B7)^*(A4^*A9^*B10 + A4^*B9^*A10^*A5^*B10^*A8 + A10^*B5*A8)]\} /[(-A1^*B6^*A3^*A1^*B2^*A7^*B1^*A2^*A7 + B1^*A6^*A3)^*(-A5^*B10^*B8 + A10^*B8^*B5^*B4^*A9^*B10 - B7^*B9^*A10) + (-A1^*B6^*B3 + A1^*B2^*B7 + B1^*A2^*B7 + B1^*A6^*B3)^*(A4^*A9^*B10 + A4^*B9^*A10 - A5^*B10^*A8 + A10^*B5^*A8)]$$

$$B_{j,1} = \{C1^*[(-A6^*A3 + A2^*A7)^*(-A5^*B10^*B8 + A10^*B8^*B5^*B4^*A9^*B10^*B7^*B9^*A10) + (-A6^*B3 + A2^*B7)^*(A4^*A9^*B10 + A4^*B9^*A10 - A5^*B10^*A8 + A10^*B5^*A8)]\} /[(-A1^*B6^*A3 - A1^*B2^*A7^*B1^*A2^*A7 + B1^*A6^*A3)^*(-A5^*B10^*B8 + A10^*B8^*B5 - B4^*A9^*B10 - B7^*B9^*A10) + (-A1^*B6^*B3 + A1^*B2^*B7 + B1^*A2^*B7 + B1^*A6^*B3)^*(A4^*A9^*B10 + A4^*B9^*A10 - A5^*B10^*A8 + A10^*B5^*A8)] \quad (C2)$$

AUTHOR INFORMATION

Corresponding Author

Chaoqun Ren − *CNOOC China Limited, Haikou 570312, China*; Email: renchq@cnooc.com.cn

Authors

Chuanzhong Deng − *CNOOC China Limited, Haikou 570312, China*

Zhehao Jiang − *CNOOC China Limited, Shanghai 200335, China*

Qiang Fu − *CNOOC China Limited, Haikou 570312, China*

Lili Jiang − *CNOOC China Limited, Haikou 570312, China*

Yuchuan Guo − *China University of Petroleum (Beijing), Beijing 102249, China*; orcid.org/0009-0005-0830-0467

Keliu Wu − *China University of Petroleum (Beijing), Beijing 102249, China*; orcid.org/0000-0002-0021-5007

Complete contact information is available at: https://pubs.acs.org/10.1021/acsomega.3c08949

Notes

The authors declare no competing financial interest.

ACKNOWLEDGMENTS

This work was supported by the Beijing Natural Science Foundation (3232029), National Natural Science Foundation of China (52174041; 52104051; 51874319), Postdoctoral Innovation Talents Support Program in China (BX20220350), and China Postdoctoral Science Foundation (2022M713459). We also would like to thank CNOOC (China) Hainan Branch for providing geological data for this study.

APPENDIX A

C_{CO_2} total mass concentration of CO_2 in the gas and water phases, mol/L
F_{CO_2} total CO_2 partial flow, mol/L
S_g gas saturation, dimensionless quantity
f_g CO_2 partial flow rate, mol/L
q gas production rate, m^3/day
B gas volume coefficient, m^3/m^3
t production time, days
φ porosity, %
A seepage cross-sectional area, m^2
x seepage length, m
L one-dimensional formation length, m
h thickness, m
R formation radius, m
K permeability, mD
P formation pressure, MPa
Krg gas phase permeability, dimensionless quantity
Krw water phase permeability, dimensionless quantity
μ_g gas viscosity, mPa·s
μ_w water viscosity, mPa·s
C_g gas compressibility, MPa^{-1}
C_w water compressibility, MPa^{-1}
C_p rock compressibility, MPa^{-1}
r_e outer boundary distance, m
R_{sw} solubility of CO_2 in water, m^3/m^3
P system pressure, 0.1 MPa
T system temperature, K

REFERENCES

(1) Sabatier, L., Dessort, D.; Madhaoui, F. Gas Reservoir Management: How to Improve Gas Production Allocation Per Reservoir in Commingled Wells Using Geochemistry Technology[C]// *International Petroleum Technology Conference*; OnePetro 2015.

(2) Huayin, Z. H. U.; et al. Physical simulation of commingled production for multilayer gas reservoir in Sebei gas field, Qaidam Basin. *Acta Petrolei Sinica* **2013**, *34*, 136.

(3) WANG, L.; YANG, S.; LIU, Y.; XU, W.; DENG, H.; MENG, Z.; HAN, W.; QIAN, K.; et al. Experiments on gas supply capability of commingled production in a fracture-cavity carbonate gas reservoir[J]. *Pet. Explor. Dev.* **2017**, *44* (5), 824−833.

(4) Long, H. N.; Yu, G. M.; Fu, X. H. New splitting method of improving the inverse distance weighted interpolation method based on grey correlation[J]. *Sci. Technol. Eng.* **2019**, *19* (36), 140−146.

(5) Lefkovits, H. C.; Hazebroek, P.; Allen, E. E.; et al. A Study of the Behavior of Bounded Reservoirs Composed of Stratified Layers[J]. *Society of Petroleum Engineers Journal* **1961**, *1* (01), 43−58.

(6) Tariq, S. M.; Ramey, H. J. Drawdown behavior of a well with storage and skin effect communicating with layers of different radii and other characteristics[C]// *PE annual fall technical conference and exhibition*; OnePetro, 1978.

(7) Shah, P. C.; Spath, J. B.. Transient wellbore pressure and flow rates in a commingled system with different layer pressures[C]// *SPE production operations symposium*; OnePetro, 1993.

(8) Jia, Y L.*Research on the theory of complicated porous flow and analysis method of well test for multilayers reservoirs[C]//* Southwest Petroleum University.2014.

(9) Fankun, M.; Yuliang, S.; Yongmao, H.; et al. Injectivity of CO_2 WAG in low permeability oil reservoirs based on B-L equations[J]. *J. China Univ. Pet.* **2018**, *42* (4), 91−99.

(10) Chang, Y. B., Coats, B. K., Nolen, J. S. A compositional model for CO2 floods including CO2 solubility in water[C]// *Permian Basin Oil and Gas Recovery Conference*. OnePetro, 1996.

(11) Kiepe, J.; Horstmann, S.; Fischer, K.; et al. Experimental determination and prediction of gas solubility data for CO2+ H2O mixtures containing NaCl or KCl at temperatures between 313 and 393 K and pressures up to 10 MPa[J]. *Industrial & engineering chemistry research* **2002**, *41* (17), 4393−4398.

https://doi.org/10.1021/acsomega.3c08949
ACS Omega 2024, 9, 12850−12865

(12) Noh, M., Lake, L W, Bryant, S L, et al. *Implications of coupling fractional flow and geochemistry for CO2 injection in aquifers.* Paper SPE 89341 presented at SPE[C]//DOE Symposium on Improved Oil Recovery, Tulsa, OK. 2004: 17−21.

https://doi.org/10.1021/acsomega.3c08949
ACS Omega 2024, 9, 12850−12865